объединенный
институт
ядерных
исследований
дубна

E1-81-289

A.Bujak, P.Devensky, E.Jenkins,[1] A.Kuznetsov, E.Malamud,[2] M.Miyajima,[2] B.Morozov, V.Nikitin, P.Nomokonov, Yu.Pilipenko, V.Smirnov, R.Yamada[2]

PROTON-HELIUM ELASTIC SCATTERING FROM 45 TO 400 GeV

Submitted to "The Physical Review D"

1) University of Arizona Tucson, Arizona 85721 USA
2) Fermi National Accelerator Laboratory Batavia, Illinois 60510 USA.

1981

I. INTRODUCTION

Previous studies of proton-helium elastic scattering have been made at low and intermediate energies[1]. Results at 24 GeV/c have been reported[2]. An experiment on the inverse reaction ^{4}He-proton elastic scattering at 1.75, 2.51 and 4.13 GeV/nucleon has also been reported[3-4]. The measurements of e^{4}He up to 1 GeV/c[5,6] and of π^--He at 7.76 GeV/c[7] are available in the literature. All these experiments exhibit a diffraction minimum or dip in the differential cross section. Such a structure is more pronounced at higher energies.

There are several theoretical models capable of describing the shape of the differential cross section[8,9]. Czyż, Leśniak, and others[10,11,12] have developed the Glauber multiple scattering model extensively. In this model the first minimum arises due to the interference between the single ($k = 1$) and multiple ($k = 2,3,4$) scattering of the incident particle inside the nucleus. The $k = 1$ and $k = 2$ imaginary amplitudes cancel at the diffraction minimum. What remains is the coherent sum of the real amplitudes for $k = 1$-4, imaginary amplitudes ($k = 3,4$), spin effects and, for $k = 2,3,4$ scattering, the amplitudes for the processes going through intermediate inelastic states. The ^{4}He is the most compact light nucleus. In the case of pHe collisions, inelastic rescattering is expected to be much larger than in another light nucleus. Thus, comparison of the results of proton-proton, proton-deuteron, and proton-helium scattering experiments is a promising way to estimate the most important corrections to the Glauber multiple scattering model.

Table I: $d\sigma/dt$ differential cross sections for elastic p^4He at 45, 97, 146, 200, 259, 301, and 393 GeV. Errors are only statistical, and the error in absolute normalization is ±4.8% as stated in text

-t [(GeV/c)^2]	dσ/dt [mb/(GeV/c)^2]	Δ(dσ/dt) statistical [mb/(GeV/c)^2]	-t [(GeV/c)^2]	dσ/dt [mb/(GeV/c)^2]	Δ(dσ/dt) statistical [mb/(GeV/c)^2]
		45 GeV			
0.00338	768.4	8.5	0.13606	6.52	0.14
0.00473	700.5	7.0	0.14215	4.95	0.09
0.00581	670.2	12.5	0.14743	3.62	0.05
0.00632	657.4	5.3	0.15208	3.22	0.10
0.00762	593.4	10.3	0.15657	2.19	0.05
0.00815	597.3	3.9	0.16394	1.73	0.03
0.01031	555.7	5.4	0.17581	0.993	0.038
0.01072	547.3	9.2	0.18113	0.686	0.014
0.01116	535.9	4.9	0.18930	0.450	0.016
0.01168	540.6	5.4	0.19243	0.334	0.016
0.01250	515.2	6.3	0.19323	0.334	0.016
0.01302	510.4	6.9	0.19824	0.256	0.015
0.01326	500.7	7.9	0.19897	0.197	0.020
0.01407	491.2	4.6	0.19910	0.189	0.019
0.01474	470.2	4.0	0.20036	0.234	0.010
0.01510	454.7	5.0	0.20094	0.162	0.019
0.01553	464.7	6.6	0.20173	0.171	0.017
0.01580	450.5	6.2	0.20181	0.100	0.011
0.01604	471.6	7.0	0.20257	0.150	0.013
0.01815	423.4	3.3	0.21260	0.0760	0.0084
0.01892	411.7	2.1	0.21345	0.0644	0.0100
0.02122	376.3	4.7	0.21349	0.0549	0.0071
0.02190	372.1	3.7	0.21489	0.0586	0.0066
0.02265	366.6	5.1	0.21630	0.0571	0.0063
0.02378	350.9	3.0	0.21717	0.0560	0.0096
0.02502	336.5	3.7	0.22033	0.0242	0.0076
0.02607	329.9	4.0	0.22110	0.0342	0.0067
0.02643	318.1	4.1	0.22336	0.0320	0.0050
0.02757	312.3	3.0	0.22473	0.0197	0.0051
0.02875	296.0	1.9	0.22747	0.0162	0.0043
0.03183	260.0	3.6	0.23129	0.0330	0.0049
0.03418	247.4	2.5	0.23546	0.0271	0.0043
0.03492	250.0	4.1	0.23636	0.0290	0.0046
0.03643	237.0	3.6	0.23860	0.0325	0.0043
0.03729	222.3	2.0	0.24011	0.0401	0.0064
0.03772	216.9	3.1	0.24294	0.0376	0.0050
0.04026	203.0	1.9	0.24370	0.0310	0.0059
0.04337	186.4	2.5	0.24583	0.0426	0.0050
0.04504	175.2	2.1	0.24667	0.0441	0.0070
0.04587	169.0	2.0	0.24680	0.0521	0.0051
0.04660	163.9	1.3	0.24760	0.0485	0.0059
0.04912	151.0	1.0	0.25434	0.0846	0.0070
0.05427	126.4	2.1	0.26101	0.104	0.007
0.05632	118.0	1.1	0.26279	0.0815	0.0083
0.05889	107.7	0.9	0.26420	0.0790	0.0072
0.06472	88.1	1.0	0.26505	0.0880	0.0090
0.06644	83.9	0.8	0.26832	0.113	0.007
0.06938	77.8	0.9	0.26919	0.105	0.008
0.07598	59.3	0.5	0.27144	0.114	0.006
0.07772	56.5	0.6	0.27830	0.127	0.008
0.08112	50.3	0.5	0.28674	0.139	0.011
0.08792	40.2	0.4	0.29404	0.165	0.004
0.08988	36.5	0.6	0.30993	0.174	0.013
0.09031	37.2	0.8	0.31765	0.191	0.005
0.09352	32.2	0.3	0.33411	0.164	0.011
0.09845	27.3	0.2	0.34121	0.183	0.006
0.10116	24.4	0.2	0.35896	0.174	0.010

-t [(GeV/c)^2]	dσ/dt [mb/(GeV/c)^2]	Δ(dσ/dt) statistical [mb/(GeV/c)^2]	-t [(GeV/c)^2]	dσ/dt [mb/(GeV/c)^2]	Δ(dσ/dt) statistical [mb/(GeV/c)^2]
0.10387	21.2	0.4	0.36624	0.172	0.005
0.10671	19.9	0.3	0.38490	0.169	0.011
0.11183	16.6	0.2	0.39255	0.141	0.004
0.12121	11.6	0.2	0.42130	0.121	0.005
0.12663	9.19	0.12	0.45942	0.0917	0.0063
		97 GeV			
.00332	773.9	14.9	.07453	59.5	0.7
.00339	744.1	14.9	.07701	55.6	0.6
.00568	667.2	6.1	.07950	50.4	0.5
.00575	663.3	11.1	.08774	37.8	0.4
.00635	623.5	8.0	.09592	27.0	0.2
.00708	606.3	6.7	.09703	26.7	0.3
.00783	614.6	7.6	.09986	24.3	0.2
.00863	588.0	5.0	.10904	17.0	0.2
.00873	571.3	8.0	.10999	16.2	0.1
.00946	568.7	7.2	.11574	12.7	0.1
.01935	562.5	6.3	.12507	8.81	.11
.01100	533.4	5.4	.13120	7.13	.09
.01125	536.3	6.1	.13926	4.79	.12
.01171	517.7	9.1	.14004	4.85	.07
.01222	503.7	5.2	.14726	3.38	.04
.01292	500.1	5.2	.16326	1.61	.04
.01474	454.6	7.9	.16615	1.28	.03
.01488	453.3	7.9	.17495	.781	.023
.01500	465.8	5.0	.17874	.674	.027
.01528	456.5	4.5	.18459	.413	.012
.01641	440.3	3.8	.19194	.267	.013
.01722	428.3	4.7	.19395	.205	.016
.01932	407.2	5.0	.20179	.110	.011
.01961	390.8	4.0	.20402	.0899	.0055
.01993	386.8	6.9	.20870	.0532	.0067
.02010	390.2	6.9	.21692	.0200	.0034
.02059	381.4	4.2	.22233	.0133	.0023
.02317	349.1	4.4	.22512	.0111	.0023
.02454	328.1	3.8	.23357	.0167	.0034
.02958	292.4	3.8	.23367	.0144	.0034
.02992	277.8	3.2	.24036	.0211	.0034
.03113	268.1	3.2	.24983	.0455	.0044
.03466	233.9	2.8	.25548	.0576	.0067
.03677	216.5	3.3	.25797	.0599	.0044
.04241	188.1	2.3	.26779	.0909	.0055
.04710	160.4	2.0	.27827	.112	.010
.04906	141.3	1.6	.28440	.129	.004
.05096	135.7	2.0	.29111	.140	.008
.05198	133.0	1.8	.29600	.152	.011
.06100	96.6	0.9	.31543	.160	.009
.07057	67.8	0.6	.33431	.149	.009
		146 GeV			
.00356	757.0	12.1	.08191	44.3	0.4
.00462	705.0	12.0	.08394	41.5	0.4
.00525	675.1	7.3	.08827	35.9	0.4
.00592	659.4	4.5	.09037	33.4	0.4
.00600	653.0	6.6	.09310	29.8	0.3
.00662	626.8	7.0	.09912	23.6	0.2
.00815	595.9	6.2	.10282	21.0	0.2
.00896	585.5	5.9	.11290	13.9	0.1
.00908	571.0	8.1	.11915	10.9	0.1
.00983	562.0	4.5	.12874	6.94	.10
.01074	541.3	3.9	.13503	5.61	.08
.01140	526.7	4.7	.15148	2.52	.03
.01168	531.5	3.7	.16149	1.55	.03
.01216	529.7	8.1	.16796	1.07	.03

$-t$ [$(GeV/c)^2$]	$d\sigma/dt$ [$mb/(GeV/c)^2$]	$\Delta(d\sigma/dt)$ statistical [$mb/(GeV/c)^2$]	$-t$ [$(GeV/c)^2$]	$d\sigma/dt$ [$mb/(GeV/c)^2$]	$\Delta(d\sigma/dt)$ statistical [$mb/(GeV/c)^2$]
.01268	505.6	3.2	.17089	.891	.022
.01338	493.8	4.5	.17992	.522	.021
.01546	462.4	3.2	.18387	.425	.022
.01584	457.6	3.3	.18983	.260	.009
.01781	420.3	3.0	.19736	.138	.009
.02001	399.6	4.5	.19951	.114	.012
.02027	388.3	2.4	.20977	.0334	.0052
.02071	383.3	4.2	.21458	.0209	.0042
.02396	345.3	4.0	.22859	.0094	.0020
.02538	328.7	3.4	.23146	.0042	.0020
.02566	330.4	2.2	.24012	.0209	.0031
.03056	271.8	3.2	.24029	.0167	.0042
.03089	271.2	2.8	.24[illegible]79	.0376	.0042
.03576	229.6	2.5	.25682	.0543	.0052
.03797	217.0	2.7	.26270	.0793	.0073
.04374	172.8	2.0	.26519	.0783	.0052
.04486	167.8	1.8	.27481	.105	.004
.05060	134.2	1.4	.23610	.108	.009
.05252	132.0	1.6	.29231	.127	.005
.05375	125.1	1.2	.29921	.144	.007
.06112	93.3	1.0	.30432	.143	.009
.06280	90.5	1.0	.31198	.148	.005
.06491	84.2	1.0	.32418	.144	.008
.07142	66.6	0.7	.33747	.147	.005
.07272	62.7	0.6	.34357	.171	.007
.07676	55.8	0.7	.36397	.147	.005
.07934	50.4	0.5	.38451	.0678	.0031
		200 GeV			
.00382	716.6	7.0	.09659	25.1	0.3
.00532	652.8	6.3	.10045	21.6	0.1
.00658	628.9	8.0	.10565	17.5	0.1
.00708	615.2	5.0	.11104	14.4	0.1
.00730	620.0	7.2	.11396	12.7	0.1
.00909	578.7	4.5	.12074	9.48	.11
.00934	563.8	5.7	.12649	7.52	.09
.01164	518.1	5.3	.13685	4.73	.09
.01248	507.5	3.7	.14296	3.56	.06
.01316	504.0	4.7	.14907	2.63	.03
.01417	476.6	4.2	.15396	2.32	.05
.01491	467.2	4.7	.16611	1.12	.01
.01585	457.5	4.2	.18420	.378	.009
.01677	434.4	2.5	.19845	.108	.012
.01794	418.8	3.3	.20236	.0727	.0085
.02036	390.9	4.2	.20512	.0648	.0064
.02124	374.9	1.9	.20646	.0410	.0064
.02443	337.1	2.3	.21375	.0200	.0031
.02544	325.4	3.0	.21781	.0076	.0021
.02684	309.5	2.7	.22599	.0151	.0051
.02835	295.3	2.7	.22739	.0110	.0045
.02976	278.7	2.9	.24052	.0217	.0036
.03108	267.0	2.5	.24231	.0317	.0036
.03245	252.4	1.6	.24498	.0323	.0036
.03584	223.8	2.0	.24933	.0502	.0061
.03856	206.4	2.2	.25350	.0543	.0046
.03948	202.4	2.5	.25735	.0666	.0061
.04123	185.0	2.2	.26196	.0756	.0046
.04248	178.4	1.7	.26647	.0877	.0052
.04543	161.8	1.3	.27592	.102	.003
.05083	136.1	2.0	.28862	.128	.007
.05265	125.8	1.0	.30169	.138	.003
.05540	114.3	1.2	.31496	.147	.007
.06145	93.4	1.2	.33124	.149	.003
.06342	86.8	0.9	.35801	.139	.003
.06645	76.7	0.7	.38482	.121	.004

$-t$ $[(GeV/c)^2]$	$d\sigma/dt$ $[mb/(GeV/c)^2]$	$\Delta(d\sigma/dt)$ statistical $[mb/(GeV/c)^2]$	$-t$ $[(GeV/c)^2]$	$d\sigma/dt$ $[mb/(GeV/c)^2]$	$\Delta(d\sigma/dt)$ statistical $[mb/(GeV/c)^2]$
.07416	58.3	0.5	.41319	.102	.003
.07851	49.7	0.4	.44397	.0722	.0031
.08315	41.3	0.5	.47632	.0519	.0032
.08693	36.0	0.3	.50900	.0298	.0032
.09155	30.5	0.2			
		259 GeV			
.00388	729.0	8.5	.10673	17.2	0.1
.00739	629.6	6.3	.11218	13.9	0.1
.00922	578.4	5.0	.11509	12.2	0.1
.00946	569.3	7.0	.12196	9.16	.12
.01277	512.6	6.6	.12777	7.19	.09
.01333	502.6	5.8	.13822	4.47	.08
.01435	488.2	5.4	.14440	3.35	.06
.01509	465.4	5.9	.15123	2.32	.04
.01605	461.4	4.7	.16204	1.41	.04
.01684	439.5	4.0	.16554	1.13	.03
.01717	438.8	4.2	.16805	1.000	.030
.02062	391.5	4.3	.18071	.430	.021
.02112	384.7	4.3	.18657	.293	.009
.02152	377.5	2.8	.20708	.0380	.0053
.02452	336.8	3.3	.20845	.0199	.0060
.02574	322.3	3.5	.21584	.0107	.0033
.02716	309.2	3.2	.21989	.0073	.0026
.02867	294.0	3.3	.22645	.0060	.0026
.03009	286.6	3.0	.22956	.0119	.0040
.03144	267.2	3.1	.23060	.0099	.0026
.03279	254.3	1.9	.24286	.0478	.0066
.03623	225.1	2.4	.24460	.0341	.0040
.03899	208.2	2.3	.24715	.0518	.0039
.03993	198.6	2.1	.25172	.0601	.0060
.04293	179.7	2.0	.25590	.0707	.0046
.04589	161.3	1.4	.25985	.0741	.0112
.04943	139.7	1.9	.26429	.0890	.0078
.05138	134.5	1.7	.26900	.0946	.0054
.05345	122.5	1.5	.27884	.115	.003
.05599	110.9	1.2	.29134	.124	.010
.06208	92.6	1.3	.30021	.150	.005
.06410	82.0	0.7	.30822	.152	.004
.06715	75.8	0.7	.31794	.143	.010
.07380	59.8	0.7	.32707	.128	.009
.07932	48.1	0.4	.33551	.152	.004
.08403	41.1	0.5	.36113	.138	.003
.08655	36.9	0.4	.38759	.115	.003
.08872	33.9	0.4	.41639	.0909	.0029
.09258	29.6	0.3	.44767	.0598	.0026
.09758	24.9	0.3	.48049	.0393	.0025
.10031	22.2	0.2	.51373	.0340	.0033
.10274	19.6	0.2			
		301 GeV			
.00385	717.8	9.5	.10185	19.7	0.1
.00666	636.9	8.0	.10701	16.4	0.2
.00715	626.4	7.1	.11244	13.1	0.1
.00738	596.0	7.1	.11534	11.6	0.1
.00863	584.4	6.1	.12224	8.49	.10
.00920	567.1	4.6	.12810	6.68	.08
.00944	560.7	5.6	.13856	4.02	.08
.01176	523.2	5.5	.14478	3.15	.06
.01243	513.9	6.1	.15102	2.24	.03
.01433	479.4	4.3	.15586	1.86	.05
.01507	464.7	4.7	.16781	.930	.013
.01605	448.5	4.3	.18660	.274	.008
.01696	434.6	2.6	.20097	.0789	.0090
.01815	419.4	3.3	.20484	.0581	.0080

-t $[(GeV/c)^2]$	$d\sigma/dt$ $[mb/(GeV/c)^2]$	$\Delta(d\sigma/dt)$ statistical $[mb/(GeV/c)^2]$	-t $[(GeV/c)^2]$	$d\sigma/dt$ $[mb/(GeV/c)^2]$	$\Delta(d\sigma/dt)$ statistical $[mb/(GeV/c)^2]$
.02062	387.6	4.4	.20764	.0529	.0047
.02147	374.1	1.9	.20900	.0351	.0070
.02473	328.4	2.3	.21646	.0039	.0024
.02576	317.9	3.0	.22049	.0024	.0019
.02716	300.9	2.7	.22713	.0119	.0033
.02869	293.0	2.7	.22876	.0085	.0047
.03010	278.1	3.1	.23020	.0127	.0047
.03148	261.2	2.5	.23124	.0123	.0033
.03263	247.7	2.4	.24358	.0378	.0048
.03626	220.5	2.1	.24528	.0454	.0043
.03902	201.9	2.3	.24784	.0464	.0039
.04172	186.6	2.3	.25242	.0647	.0075
.04298	174.2	1.7	.25662	.0761	.0057
.04595	157.2	1.1	.26062	.0743	.0071
.04951	138.5	2.0	.26502	.0805	.0058
.05144	128.1	1.8	.26977	.0915	.0058
.05328	122.5	1.0	.27891	.110	.003
.05607	109.8	1.1	.29217	.130	.006
.06217	88.2	1.1	.30544	.142	.003
.06413	82.0	0.8	.31887	.140	.007
.06727	72.4	0.6	.33514	.139	.003
.07509	55.2	0.4	.36251	.122	.003
.07948	46.8	0.4	.38898	.0980	.0032
.08421	39.2	0.4	.41760	.0822	.0028
.08671	35.0	0.3	.44944	.0551	.0025
.08943	31.3	0.5	.48243	.0428	.0027
.09271	28.7	0.2	.51534	.0332	.0034
.09781	23.4	0.2			
			393 GeV		
.00385	720.9	10.1	.10392	18.4	0.4
.00718	639.8	7.4	.10746	16.0	0.1
.00922	597.7	6.0	.11293	12.9	0.2
.00948	591.6	8.7	.11591	11.4	0.1
.01180	540.1	6.7	.12291	8.56	.19
.01278	511.0	7.7	.12867	6.68	.09
.01335	512.1	7.0	.13920	4.10	.09
.01439	495.9	6.5	.14543	3.14	.07
.01513	490.9	7.2	.15118	2.16	.04
.01609	466.3	5.7	.16322	1.21	.05
.01702	451.2	3.4	.16920	.809	.018
.01804	437.6	5.5	.18205	.415	.024
.02067	399.1	5.1	.18805	.247	.009
.02160	377.2	2.6	.20191	.0625	.0118
.02483	342.9	3.0	.20589	.0441	.0085
.02584	328.5	4.1	.20869	.0284	.0088
.02727	315.0	3.7	.21004	.0100	.0079
.03023	285.3	3.5	.21750	.0073	.0060
.03158	267.4	3.5	.22162	.0092	.0053
.03295	253.7	2.2	.22821	.0193	.0053
.03641	225.4	2.7	.22994	.0125	.0066
.03917	208.5	2.7	.23134	.0183	.0081
.04190	186.2	2.1	.23242	.0132	.0046
.04317	177.6	2.3	.24475	.0384	.0074
.04614	160.1	1.5	.24654	.0542	.0053
.04970	138.6	2.2	.24913	.0539	.0061
.05167	128.1	1.9	.25369	.0808	.0079
.05339	121.8	1.1	.25795	.0824	.0067
.05631	113.1	1.4	.26189	.0985	.0141
.06247	89.6	1.5	.26641	.0957	.0107
.06475	81.9	1.0	.27861	.116	.003
.06757	75.2	0.8	.29370	.121	.012
.07428	58.1	0.8	.30707	.142	.004
.07642	52.6	0.7	.32051	.142	.013
.07983	46.0	0.5	.33723	.141	.004

$-t$ $[(GeV/c)^2]$	$d\sigma/dt$ $[mb/(GeV/c)^2]$	$\Delta(d\sigma/dt)$ statistical $[mb/(GeV/c)^2]$	$-t$ $[(GeV/c)^2]$	$d\sigma/dt$ $[mb/(GeV/c)^2]$	$\Delta(d\sigma/dt)$ statistical $[mb/(GeV/c)^2]$
.08456	40.1	0.5	.36412	.127	.004
.08713	35.6	0.4	.39096	.101	.004
.08933	32.4	0.5	.42034	.0787	.0033
.09313	28.2	0.3	.45154	.0561	.0030
.09823	23.0	0.3	.48476	.0382	.0029
.10101	20.7	0.3	.51808	.0268	.0034

In Section II we describe the experiment and details of the analysis. The method of absolute normalization of the differential cross section is presented in Section III. In Section IV and Table I we present our proton-helium data at 45, 97, 146, 200, 259, 301 and 393 GeV. The 45 GeV data was originally taken as two separate experiments at 44.9 GeV and 45.5 GeV. In the differential cross sections shown in Table I these two sets of data have been averaged. The figures and tables derived from fits to the differential cross sections preserve these data as two independent points and illustrate the reproducibility of the data.

The results of the fits to the low $|t|$ region are discussed in Section V. The tables with a list of parameters include the slope $b(s)$, the t-dependence of the slope, the real part of the amplitude at $|t| = 0$, the total p^4He cross section, and the s-dependence of all the above parameters using a linear approximation. In Section VI we compare the Glauber model predictions to the data in the entire t region including the diffraction dip. In Section VII we summarize the results.

II. EXPERIMENTAL APPARATUS AND DATA ANALYSIS

The experimental apparatus is shown in Fig. 1. The Fermilab circulating proton beam intercepts a gas target with

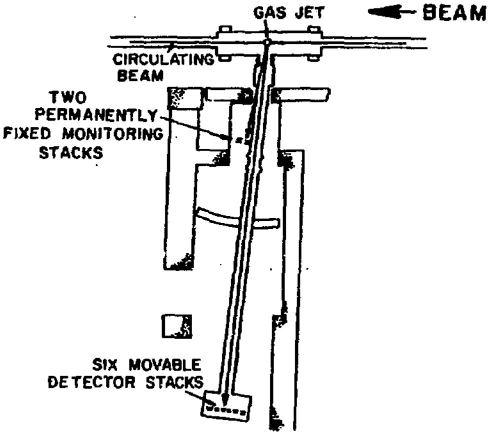

Figure 1: Schematic representation of the apparatus.

an average thickness of 4×10^{-7} g/cm^2 and a jet width (r.m.s.) of ±3 mm. The gas jet pulse length is 100 msec and occurs at two energies during the accelerator ramp cycle. During the "live time" of the gas jet the value of the actual beam energy is written into the computer every 40 msec. The variation of primary energy over the jet pulse length is ±8 GeV or less depending on the accelerator rate of rise.

Helium is injected into a 250 liter buffer volume, and 90% of the gas is removed by a 5000 liter/sec diffusion pump. The remainder is removed from the accelerator vacuum chamber by 8 diffusion pumps spaced at 5 m intervals upstream and downstream from the target. These pumps constitute a differential pumping system and reduce the helium partial pressure to 10^{-9} mm Hg beyond the last upstream and downstream pumps.

The target is viewed at near 90° by sets of stacks of solid state detectors. Each stack consists of two silicon detectors with typical dimensions of 5 x 30 mm^2. The thickness of the front detectors ranges from 15μm to 250 μm and of the back detectors from 200 μm to 1500 μm. The detectors have a noise of 50 KeV and energy resolutions of 50-150 KeV. The 6 movable stacks are installed at 7.2 m from the target inside of the vacuum chamber, which together with the "ion-guide" connecting it with the target chamber forms a remotely movable arm. The range of laboratory angles covered by the detectors is 84.5^{o} - 89.7^{o} (relative to the beam direction). The relative position of the detector arm is measured with accuracy ±0.02 mrad; the relative angles between stacks are known with accuracy ±0.025 mrad and remain constant for the whole experiment.

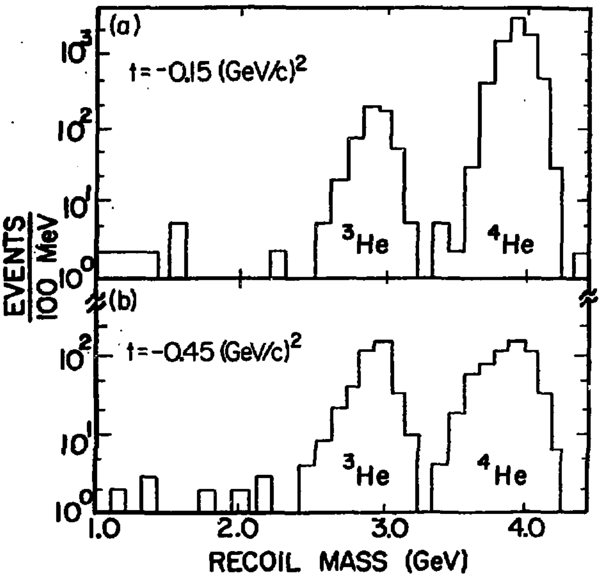

Figure 2: Mass distribution obtained from the two-dimensional plot using relation (1). The peaks corresponding to isotopes ^{3}He, ^{4}He are shown.

The 7.2 m distance from the target and the detector dimensions yields a geometric resolution of $\Delta\theta = \pm 0.7$ mrad. The resulting kinetic energy uncertainty $\Delta T/T = 2\ \Delta\theta/\theta$, where θ is the recoil angle with respect to 90^o, is good enough to provide separation between the elastic and inelastic reactions. Two additional permanently fixed stacks are used to monitor the jet-beam interaction rate. During readout of a stack, the inputs to all other stacks are inhibited. Thus, all channels have the same dead time percentage (3%). A typical counting rate is about 1000 events per beam spill distributed over 8 stacks.

The $|t|$ interval studied is $.003 \leq |t| \leq 0.52\ (GeV/c)^2$ corresponding to recoil angles of $6 < \theta < 96$ mrad and ranges of $2 < R < 1800\ \mu m$ in silicon. The multiple scattering of the outgoing recoil particle in the target gas is negligible except at the smallest $|t|$ values. In the worst case, at $|t| = .003\ (GeV/c)^2$, the multiple scattering mainly affects the energy resolution but the corrections to the cross section are smaller than 1%.

The detectors are calibrated against a $^{234}_{90}Th$ alpha particle source. When compared with survey measurements, the absolute angles determined from the elastic peak show an offset difference of 0.3 mrad; this is consistent with the absolute angular uncertainty estimated to be less than ± 0.2 mrad. The magnetic field action on the recoils is reduced by shielding to ≤ 0.03 gauss in order to minimize angular errors at low $|t|$. At $|t| = .003\ (GeV/c)^2$ the remaining field can cause at most an angular change of ≤ 0.12 mrad.

The first step in the analysis is to separate coherent ^4He recoils from H, D, T, ^3He. The energies in MeV deposited in the detector sandwiches are sorted into 256 x 256 plots of the front detector T_F versus the back detector T_B. The mass of a ^{4}He particle stopping in the back element is deduced from the known range-energy relation and is given by the empirical formula:

$$m = m_p \left[\frac{\alpha}{d_F Z^2} \left| (T_F + T_B)^{\beta} - T_B^{\beta} \right| \right]^{1/(\beta - 1)} \quad (1)$$

where $\alpha = 13.3$, $\beta = 1.73$, and d_F is the thickness of the front detector in mm. In Fig. 2a and b we plot the recoil mass distribution for $t = -0.149$ and -0.450 $(GeV/c)^2$ respectively. The ^{4}He, ^{3}He mass separation is excellent at these $|t|$ values.

For the separated ^{4}He recoils the momentum spectra are obtained and described by a formula which contains Gaussian plus polynomial background terms. The number of elastic scattering events is calculated as the sum over the peak within the limit $\pm 4\sigma$. The number of background events under the elastic peak is usually 1-3% except for the region of the diffraction minimum. In the dip region, $t = -0.22$ $(GeV/c)^2$, the p^{4}He elastic cross section drops 5 orders of magnitude, and the systematic uncertainty is about $\pm 50\%$ due to inelastic background subtraction.

The results from an analysis of the inelastic p^{4}He are presented in the accompanying paper[13] on coherent proton diffraction dissociation of helium from 45 to 400 GeV.

III. ABSOLUTE NORMALIZATION

The ratios of the proton-helium to the proton-hydrogen differential cross sections have been obtained from auxiliary measurements using a hydrogen/helium mixture as a target. Three of the movable stacks and one of the two fixed monitoring stacks are used to observe pp elastic scattering. The other half of the detector stacks are used to see pHe elastic scattering.

The absolute value of $d\sigma_{pHe}/d\omega$ is calculated from the relation

$$\frac{d\sigma_{pHe}}{d\omega} = \frac{n_{He}}{n_p} \frac{\Delta\omega_p}{\Delta\omega_{He}} \frac{k_p}{k_{He}} \frac{d\sigma_{pp}}{d\omega} \tag{2}$$

where n is the number of elastic scattering events, $\Delta\omega$ is the solid angle of the stack, k is the atomic concentration of gas and $d\sigma_{pp}/d\omega$ is the known differential cross section for elastic pp scattering. The auxiliary experiment has been done at 9 energies: 49, 66, 90, 161, 200, 258, 280, 301 and 393 GeV in a range $0.001 < |t| < 0.02$ for pp and $0.007 < |t| < 0.11$ $(GeV/c)^2$ for pHe. Since this is a new technique there are a number of concerns we have about possible systematic errors. The mixture ratio could change as the gas emerged from the gas jet nozzle. To examine this possibility we looked for possible time structure in the ratio, n_{He}/n_p within the 100 msec spill. We also compared the shape and width of the hydrogen and helium jets obtained by unfolding them from the elastic pulse height distribution using elastic kinematics. No differences were seen.

To look for longer term time variation we plotted the ratio of the number of detected elastic events for pp and pHe collisions from run to run for the two fixed stacks. This ratio remains constant during the data collection time of about 30 hours (16 independent runs). We conclude that the ratio of luminosities of the partial targets (hydrogen and helium) is independent of time.

An additional check of this technique has been performed using a hydrogen-deuterium mixture as a target. In this case both differential cross sections are known. From the measured ratio n_p/n_d we deduce the absolute value of the differential pd cross section and, using the optical theorem, calculate the total cross section for pd interactions: $\sigma_{tot}(pd) = 73.24 \pm 0.47$ mb at E = 49 GeV and 74.61 ± 0.47 mb at E = 259 GeV. This is in good agreement with the data by Carrol et al.[14]

The auxiliary experiment with a hydrogen-helium mixture has been done at a limited number of angular points. The data obtained are used only for absolute normalization of the relative cross sections measured in the course of the main experiment.

Normalization is done as follows. Using a starting value for the total cross section, fits are done to the data of the main experiment by techniques described in Section IV. Once parameters describing the shape of the differential cross section are found the mixture data is used to find the correct normalization for the main experiment. With normalization now fixed, a new fit is done to the main experiment data and iteration continued until the parameters are stable. Since the energy of the primary beam in these two sets of measurement is slightly different, corresponding interpolation is done.

Results are shown in Fig. 3. The errors shown are only statistical. The systematic error is hard to estimate given some of the problems discussed above. The hydrogen/helium mixture is 48.33%/51.56%. This ratio is known with a precision of ±4%. The corresponding uncertainty in σ_{tot}^{pHe} is ±2.5 mb. There are two additional sources of systematic uncertainty in σ_{tot}^{pHe}. Background subtraction in the mixture experiment contributes an uncertainty of ±1.5 mb. Extrapolation to the optical point depends on the model used. If, e.g.,

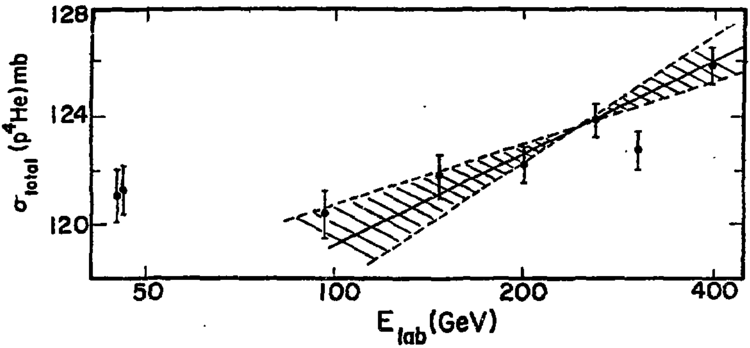

Figure 3: Total cross section for p^4He interactions. The straight line is calculated according to the geometric scaling relation, σ_{tot} proportional to b, the slope parameter (see Table IV). The dashed area is the one standard deviation corridor uncertainty.

we use the parameterization of Schiz et al[15] instead of the pp parameterization we have used this lowers σ^{pHe}_{tot} by about 1.7 mb. The total systematic error in σ^{pHe}_{tot} is then estimated as ±3 mb.

After this paper was written preliminary results from a new CERN experiment became known to us.[16] Since they use an external beam and a conventional target they, in principal, can determine their normalization more accurately. Of course to obtain σ^{pHe}_{tot} one must assume a shape for the differential cross section and extrapolate to t = 0. Their preliminary total cross section is 8-9 mb higher than ours; their quoted total error is ±0.8 mb. The amusing part is that these preliminary CERN results agree with our preliminary results, presented at the Tokyo conference[17]. In that case we normalized using the differential cross section in the Coulomb interference region. Although it gave statistical accuracy comparable to this paper we feel the mixture technique is inherently more reliable than the Coulamb technique because in that case the value obtained depends critically on the cross section shape used.

The main virtue of our measurements lies in the wide range of s- and t- covered with one experimental setup. It is a simple matter at a later date, if necessary, to renormalize the data in Table I and refit to any desired model.

IV. DIFFERENTIAL CROSS SECTIONS

The differential cross sections for p^4He elastic scattering are given in Table I. The errors listed are statistical only. Examples of the differential cross section, $d\sigma/dt$, are shown in Figs. 4a and b. The general characteristics of the data are a differential cross section which drops 4-5 orders of magnitude to a first dip at $|t| \approx 0.22\ (GeV/c)^2$ and a subsequent rise to a secondary maximum at $|t| \approx 0.33\ (GeV/c)^2$.

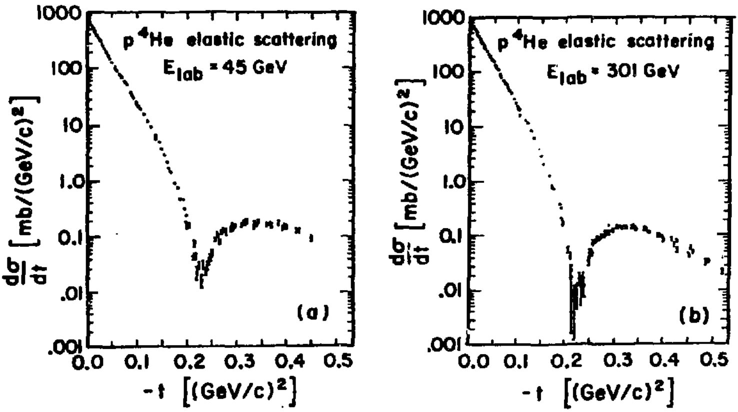

Figure 4: Examples of the differential cross section of p^4He elastic scattering: (a) $E_{lab} = 45$ GeV, (b) $E_{lab} = 301$ GeV.

Table II: Systematic errors in $d\sigma/dt$

	Dependent on t	Dependent on E_{lab}	Lowest $\|t\|$		Highest $\|t\|$		Dip Region	
			Lowest E_{lab} ±%	Highest E_{lab} ±%	Lowest E_{lab} ±%	Highest E_{lab} ±%	$t_{min}=-.24$ Lowest E_{lab} ±%	$t_{min}=-.22$ Highest E_{lab} ±%
Collimator area	No	No	0.5	0.5	0.5	0.5	0.5	0.5
Monitor (statistical error)	No	No	1.0	1.0	1.0	1.0	1.0	1.0
Absolute angular scale uncertainty ±0.2 mrad	Yes	No*	0.3	0.3	0.3	0.3	2.0	2.0
Magnetic field	Yes	No	0.1	0.1	0	0	0	0
Background (residual gas)	No	No	0.3	0.3	0.3	0.3	0.3	0.3
Inelastic background	Yes	Yes	0.0	0.0	0.0	3.0	0.0	50.0
Absolute normalization	No	No	5.4	5.4	5.4	5.4	5.4	5.4
Total			5.5	5.5	5.5	6.3	5.9	50

*Systematic error depends on the depth of the dip region.

Table III: Total elastic cross section, position and height of the second maximum. The systematic error in $\sigma_{tot\ el}$ is ±0.62 mb

E_{lab} GeV	$\sigma_{tot\ el}$ (mb)	$-t_{sec.max}$ $[(GeV/c)^2]$	$(d\sigma/dt)_{sec.max}$ $[mb/(GeV/c)^2]$
45	23.09 ± 0.23	0.319	0.190 ± 0.015
46	22.80 ± 0.23	0.318	0.184 ± 0.016
97	22.26 ± 0.22	0.321	0.160 ± 0.010
146	22.37 ± 0.22	0.328	0.167 ± 0.010
200	22.18 ± 0.22	0.324	0.166 ± 0.010
259	22.54 ± 0.23	0.326	0.150 ± 0.016
301	22.11 ± 0.22	0.327	0.153 ± 0.012
393	22.93 ± 0.23	0.333	0.147 ± 0.010

The sources of systematic errors and their variation with E_{lab} and t are listed in Table II. These systematic errors are errors on the individual data points; an additional error in the overall normalization must be added. The statistical error of absolute normalization is ±0.7%, the systematic uncertainty is ±4.8% as explained above. Thus the total error in absolute normalization of the differential cross sections given in Table I is ±4.8%.

Table III lists values of the total elastic p^4He cross sections. They are obtained by integration of the differential cross section in the t-range $0 \leq |t| \leq 0.5$ $(GeV/c)^2$ after Coulomb and Coulomb-nuclear interference effects are subtracted. Another general characteristic of the differential cross section is the position and the magnitude of the second maximum. They are given in Table III as well.

V. SMALL t REGION

The results for the p^4He elastic cross section, listed in Table I, are described in the range $0.003 \leq |t| \leq 0.11$ $(GeV/c)^2$ by the Bethe interference formula[18]

$$\frac{d\sigma}{dt} = \left| f_c \cdot e^{i\phi} + f_n \right|^2 , \qquad (3)$$

where the Coulomb scattering amplitude takes the form

$$f_c = \frac{4\alpha\hbar\sqrt{\pi}}{t} G_p(t) \, G_{He}(t) \; . \qquad (4)$$

Here α is the fine structure constant, $\phi = 4\alpha \ln \frac{1.06\hbar}{R\sqrt{|t|}}$ is the Coulomb phase, $R = \sqrt{\frac{2}{3}} < R_{He}{}^2 >^{1/2}$ is the ^4He electromagnetic radius[5,6] ($R_{He} = 1.67$) derived from e^4He scattering, $G_p(t) = (1 - t/0.71)^{-2}$ is the proton electromagnetic form factor, and $G_{He}(t) = \left[1 - (2.56t)^6\right] \times e^{11.70t}$ is the ^4He electromagnetic form factor.[5,6] The nuclear scattering amplitude takes the form

$$f_n = \frac{\sigma_{tot}^{pHe}}{4\hbar\sqrt{\pi}} \, (i + \rho) \cdot e^{\frac{bt+ct^2}{2}} , \qquad (5)$$

where σ_{tot}^{pHe} is the total proton-helium cross section, $\rho = \left.\frac{Ref}{Imf}\right|_{t=0}$ is the ratio of the real to the imaginary part of the forward scattering amplitude, and *b*,c are the linear and quadratic slope parameters.

The results of the fit in the range $0.003 < |t| < 0.11$ $(GeV/c)^2$ are listed in Table IV. The fitted parameters are σ_{tot}^{pHe}, the proton helium total cross section, ρ, b, and c. The values given for σ_{tot}^{pHe} in Table IV are directly related to the normalization obtained from the mixture analysis. In Fig. 3 we show the Table IV proton-helium total cross sections at 45, 46, 97, 146, 200, 259, 301, and 393 GeV. Since the quadratic slope parameter $c \approx 22(GeV/c)^{-4}$ is energy independent within errors, an alternate fit with c fixed is listed in Table V.

Table VI presents the average slope parameter in different t intervals $0.003 < |t| < 0.007$ $(GeV/c)^2$, $0.03 < |t| < 0.1$

Table IV: The parameters of Bethe's formula Eqs. (3)-(5) describing the differential cross section for elastic p^4He scattering in an interval $0.003 \leq t \leq 0.11$ $(GeV/c)^2$

E_{lab} GeV	σ_{tot}^{pHe} (mb)	ρ	b $[(GeV/c)^{-2}]$	c $[(GeV/c)^{-4}]$	χ^2/# of points
45	121.1 ± 1.0	-0.056 ± 0.030	31.4 ± 0.4	-25.0 ± 3	81/72
46	121.4 ± 0.9	-0.012 ± 0.032	32.0 ± 0.4	-18.6 ± 3	56/60
97	120.3 ± 0.9	-0.053 ± 0.026	32.1 ± 0.3	-23.2 ± 3	98/57
146	121.8 ± 0.8	-0.024 ± 0.024	32.5 ± 0.3	-24.7 ± 3	100/71
200	122.3 ± 0.7	+0.041 ± 0.023	32.9 ± 0.3	-25.3 ± 2	59/73
259	123.9 ± 0.7	+0.046 ± 0.031	33.5 ± 0.3	-21.1 ± 3	55/60
301	122.8 ± 0.7	+0.042 ± 0.030	33.4 ± 0.3	-24.4 ± 3	58/65
393	125.9 ± 0.6	+0.102 ± 0.035	34.2 ± 0.4	-20.6 ± 3	54/64
systematic error	± 2.4%	± 0.05	± 0.16	± 0.7	

$(GeV/c)^2$ and $0.06 < |t| < 0.13$ $(GeV/c)^2$ calculated as $b_{t=t_0} = b + 2ct_0$ where b and c have been fitted in each interval. Fig. 5 shows the slope parameter b as listed in Table VI. The rate of shrinkage weakly depends on t; for energies E > 100 GeV the rate of shrinkage is t-independent (see dashed lines on Fig. 5).

Finally to complete our analysis using the Bethe formula, the s-dependence of the b, σ_{tot}^{pHe}, ρ values given in Table V have been parameterized in the form $P_i = A_i + B_i \ln(s_{pHe}/s_o)$ with $s_o = 1$ GeV^2. These results are given in Table VII. The energy dependence of ρ is plotted in Fig. 6.

The parameters $\rho(s, t=0)$ and $b(s, t)$ of the pHe scattering amplitude obtained show a rate of shrinkage of the pHe

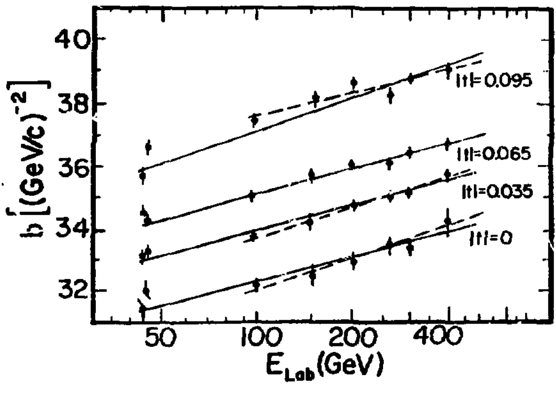

Figure 5: Average slope parameter of the diffraction peak of p^{4}He elastic scattering at different t intervals (values from Table VI). The solid lines are fits over the entire energy range. The dashed lines correspond to the fit for energies $E \geq 100$ GeV.

Table V: The same as in Table IV but with $c = -22$ $(\mathrm{GeV}/c)^{-4}$ a fixed parameter

E_{lab} GeV	σ_{tot}^{pHe} (mb)	ρ	b	$\chi^2/\#$ of points
45	121.33 ± 0.59	-0.068 ± 0.032	31.71 ± 0.10	82/72
46	120.32 ± 0.60	-0.063 ± 0.025	31.55 ± 0.11	56/60
97	120.49 ± 0.56	-0.065 ± 0.021	32.32 ± 0.09	110/57
146	121.97 ± 0.43	-0.036 ± 0.018	32.74 ± 0.08	101/71
200	122.80 ± 0.29	-0.035 ± 0.017	33.2[illegible] ± 0.08	62/73
259	123.62 ± 0.37	+0.010 ± 0.024	33.39 ± 0.09	56/60
301	123.22 ± 0.31	+0.038 ± 0.022	33.71 ± 0.08	62/65
393	125.78 ± 0.31	+0.067 ± 0.027	34.07 ± 0.10	54/64

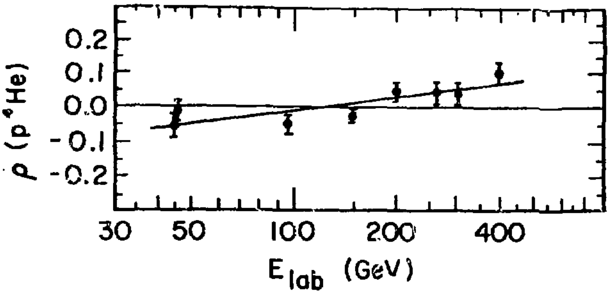

Figure 6: $\rho = \mathrm{Re}(f)/\mathrm{Im}(f)$ $(t = 0)$ for p^4He elastic scattering. The values are from Table IV. The straight line fit shows the parameterization listed in Table VII.

diffraction cone $b_1(t) = \frac{\partial}{\partial \ln s} b(s, t)$ more than twice as large as that for pp scattering.[19] This effect is in qualitative agreement with the expectation based on the Glauber model provided the screening correction is energy-dependent.[20] The other consequence of this model is the increase of the rate of shrinkage $b_1(t)$ when $|t|$ increases. This prediction is not supported from the present experiment since b_1 shows no t-dependence (see Fig. 5 and Table VI).

In Tables III and IV, and Fig. 3 we test two interesting predictions of geometric scaling. Geometric scaling, $\sigma_{tot}(E)$ proportional to $b(E)$, is satisfied (Fig. 3), but the other geometrical relation for the height of the second maximum, $\frac{d\sigma}{dt}(E, t_{sec.max})$ proportional to $\sigma_{tot}^2(E)$, is strongly violated since the function $\frac{d\sigma}{dt}(E)\Big|_{sec.max}$ decreases and the function $\sigma_{tot}(E)$ rises with E.

Table VI: Average slope parameter -- three different t intervals

E_{lab} GeV	$0.003 < \|t\| < 0.07$		$0.03 < \|t\| < 0.1$		$0.06 < \|t\| < 0.13$	
	$b\|_{\|t\|=0.035}$	χ^2/D.F.	$b\|_{\|t\|=0.065}$	χ^2/D.F.	$b\|_{\|t\|=0.095}$	χ^2/D.F.
45	33.13 ± 0.12	60/55	34.48 ± 0.14	33/26	35.63 ± 0.28	33/20
46	33.23 ± 0.13	40/47	34.24 ± 0.15	17/21	36.59 ± 0.25	21/13
97	33.55 ± 0.13	75/40	34.90 ± 0.13	41/17	37.35 ± 0.17	24/15
146	34.18 ± 0.10	61/52	35.60 ± 0.10	58/20	38.16 ± 0.14	61/22
200	34.68 ± 0.09	44/52	36.06 ± 0.09	19/30	38.57 ± 0.13	15/24
259	35.06 ± 0.10	35/42	36.11 ± 0.11	32/27	38.28 ± 0.14	31/27
301	35.16 ± 0.09	39/46	36.43 ± 0.10	30/29	38.87 ± 0.13	28/27
393	35.66 ± 0.12	35/44	36.75 ± 0.12	30/30	39.09 ± 0.17	13/21

VI. GLAUBER MODEL ANALYSIS

Data from the whole t-region, $0.003 \leq |t| \leq 0.52$ $(GeV/c)^2$, were compared and fitted to the multiple nucleon scattering model, the Glauber model. In this model the full scattering amplitude is a coherent sum of single, double, triple, and quadruple scatterings from the four nucleons in ^4He.

Table VII: Energy dependence of the b, σ_{tot}, and ρ parameters. Parameterization in the form $P_i = A_i + B_i \ln(s_{pHe}/s_o)$, with $s_o = 1\ \mathrm{GeV}^2$

Parameter	A_i	B_i	χ^2/D.F.
$b_{t=0}$ $(\mathrm{GeV/c})^{-2}$	24.8 ± 1.3	1.13 ± 0.18	4/6
$b_{t=0}$ $c=-22$ $(\mathrm{GeV/c})^{-4}$ fixed	24.9 ± 0.3	1.14 ± 0.04	10/6
$b_{t=0.035}$ $(\mathrm{GeV/c})^{-2}$	26.2 ± 0.4	1.17 ± 0.05	15/6
$b_{t=0.065}$ $(\mathrm{GeV/c})^{-2}$	26.6 ± 0.4	1.14 ± 0.06	7/6
$b_{t=0.095}$ $(\mathrm{GeV/c})^{-2}$	28.6 ± 1.0	1.32 ± 0.10	23/6
σ^{pHe}_{tot} (mb)	108.7 ± 2.8	2 [illegible] ± 2.8	14/6
$\rho_{t=0}$	-0.41 ± 0.1	0.059 ± 0.014	7/6

In our analysis we have assumed that the nucleon-nucleon scattering amplitude is spin independent and the proton-proton and proton-neutron amplitudes are equivalent. Coulomb effects are neglected for $|t| > 0.05$ $(\mathrm{GeV/c})^2$. We use a non-correlated internal (or center-of-mass) wave function for the ^{4}He nucleus and identical one-particle density distributions for the protons and neutrons. No inelastic intermediate states are included in the parameterization.

Many of the details and parameter definitions are placed in the Appendix. The values of the parameters are listed in Table IX. Two versions have been developed. For both of them comparison with the experimental data in the entire t-range is done. In Version I we calculated the nuclear amplitude in the simplest way identical with that described in ref. 10. The phenomenological analysis of its parameters is performed in the small t-range. The more complex parameterization is done in Version II.

Version I

In the small t-region the data may be successfully fitted with the following restrictive assumptions:

$$f_{\text{nucleon}} = \frac{\sigma_{\text{tot}}}{4\pi}\, p \left[i + \rho \right] e^{-\frac{b}{2} q^2} \quad \text{nucleon-nucleon amplitude}, \qquad (6)$$

$$\rho_i(\vec{r}_i) = \frac{e^{-r_i^2/R_1^2}}{\pi^{3/2} R_1^3} \quad \text{nucleon particle density}, R_1 = 1.36 \text{ fm} . \qquad (7)$$

The fitted parameters are b = slope parameter, ρ = ratio of the real to imaginary parts of the forward scattering amplitude, and σ_{tot} = the total nucleon-nucleon cross section; p is the proton laboratory momentum. We restrict the analysis

Table VIII: Parameters of the NN elastic scattering amplitude as fitted by the Glauber model, Version I, $|t| \leq 0.07$ $(\text{GeV/c})^2$. σ_{tot} pp is listed for comparison (from ref. 14). Energy dependent fits to the values of ρ and b are shown

E_{lab} GeV	$\rho_{\text{pp G1}}$	$b_{\text{pp G1}}$ $\left[(\text{GeV/c})^{-2}\right]$	$\sigma_{\text{tot G1}}$ (mb)	$\sigma_{\text{tot pp}}$ (mb)	χ^2/D.F.
45	-0.087 ± 0.028	11.27 ± 0.14	35.22 ± 0.22	38.36	60/57
46	-0.062 ± 0.032	11.31 ± 0.16	35.08 ± 0.22	38.35	40/50
97	-0.090 ± 0.027	11.89 ± 0.14	34.78 ± 0.22	38.38	76/44
146	-0.049 ± 0.024	12.29 ± 0.12	35.31 ± 0.15	38.64	62/55
200	-0.022 ± 0.022	12.76 ± 0.12	35.45 ± 0.08	38.97	46/55
259	+0.024 ± 0.030	13.03 ± 0.13	35.88 ± 0.10	39.32	34/45
301	+0.031 ± 0.029	13.20 ± 0.12	35.58 ± 0.09	39.56	38/49
393	+0.067 ± 0.036	13.47 ± 0.16	36.38 ± 0.08	40.04	44/47

$\rho_{\text{pp G1}} = -0.400 \pm 0.079 + (0.068 \pm 0.014) \ln (s_{pp}/s_0)$ $\qquad s_0 = 1 \text{ GeV}^2$

$b_{\text{pp G1}} = 6.63 \pm 0.38 + (1.03 \pm 0.07) \ln (s_{pp}/s_0)$

range to $|t| < 0.07$ $(GeV/c)^2$. The results of these fits are given in Table VIII. For comparison the values from the proton-proton experiment[17] are listed as well. In Fig. 7 the differential cross section at 393 GeV is shown. The fitted curve agrees well with the data but at the expense of increasing b, and decreasing σ_{tot} from the known nucleon-nucleon values. The curve extrapolated into the wider t-

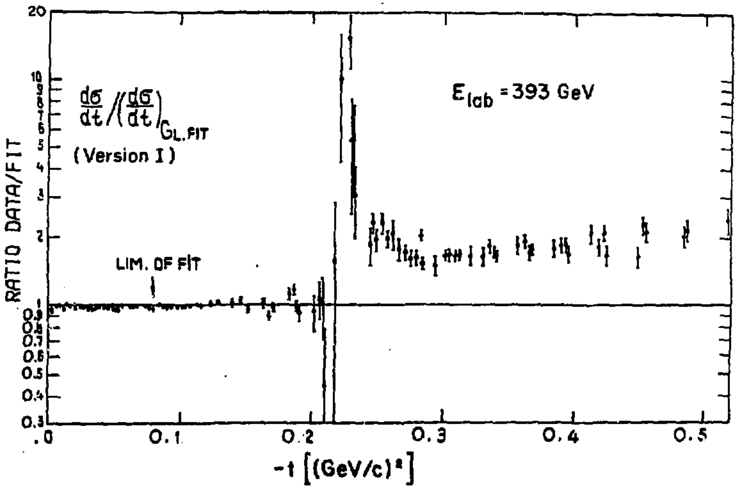

Figure 7: The elastic differential p^4He cross section at 393 GeV. The solid line is the Glauber model prediction; the simplest form of the elementary amplitude and one-particle density has been used (Version I in the text). The Coulomb effect for $-t < 0.03$ $(GeV/c)^2$ is extracted. The data fit is over the range $0.003 \leq |t| \leq 0.07$ $(GeV/c)^2$. The data is plotted as a ratio of the differential elastic cross section to that of the Glauber model prediction.

interval does not agree with the data in the region $|t| \geq 0.22$ $(GeV/c)^2$. A similar discrepency in the secondary maximum has been observed at lower energies[1,2], and interpreted by some

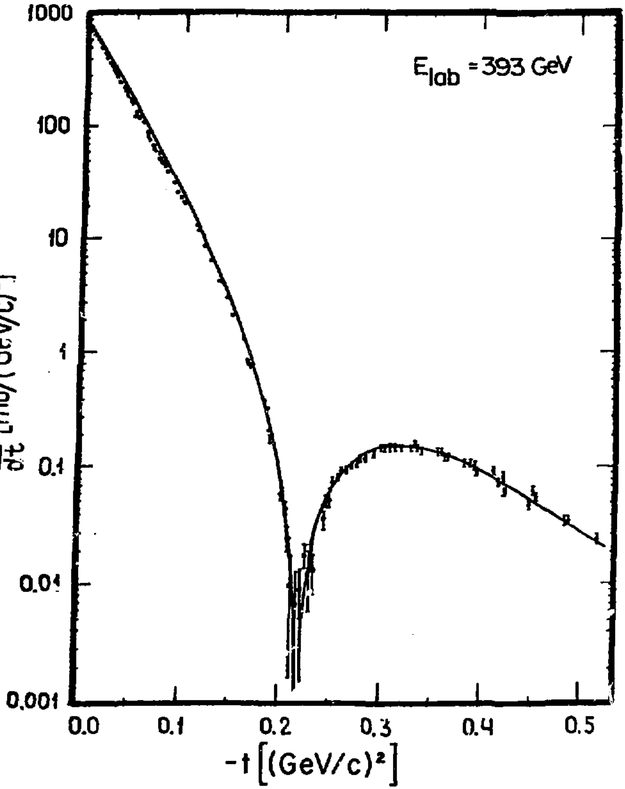

Figure 8: The elastic differential p^4He cross section at 393. σ_{tot}, b, ρ have been taken from pp experiments[17, 21] and listed in Table IX. The solid line is the Glauber model prediction with these parameters (Version I). The Coulomb effect for $|t| < 0.03$ $(GeV/c)^2$ is extracted.

authors[9] as a consequence of a non-realistic form of the wave function (Eq. 7).

Using the same formalism we calculate the differential cross section with fixed σ_{tot}, b and ρ parameters taken from pp experiments. As an illustration Figs. 8, 9 and 11 show our *393, 45 and 301 GeV data compared with corresponding curves.* This qualitative shape of the data is reproduced with a deep minimum and a secondary maximum, but the discrepancy between the data and theory is large at all energies, especially in the small t-region. A normalization change upwards would lessen this discrepancy.

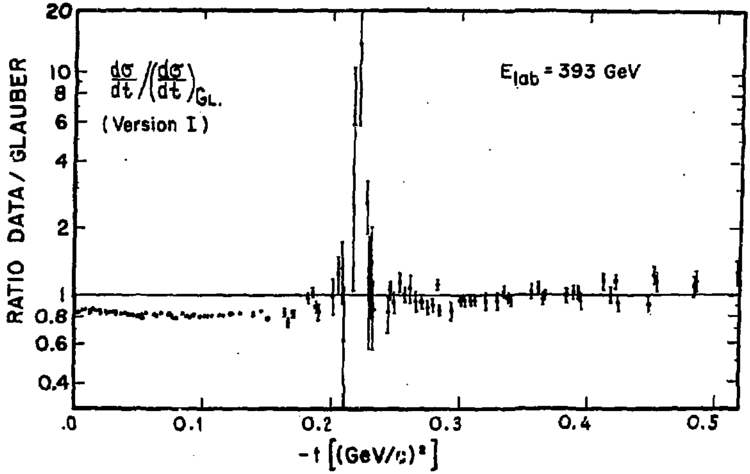

Figure 9: The elastic differential cross section at 393 GeV shown as a ratio to the Glauber model prediction (Version I). σ_{tot}, b, ρ values are those used with Figure 8.

Table IX: The parameters used in the calculation of $\frac{d\sigma}{dt}$ (p^4He). The corresponding curves are shown in Figs. 8, 9 and 11

Version	One-particle density (Eq. A5)				Elementary amplitude (Eq. A3)							
	R_1^2 (GeV^{-2})	R_2^2 (GeV^{-2})	C	References	Energy (GeV)	σ_{tot} (mb)	ρ_0	ρ'	γ (GeV^{-2})	β	b_1 (GeV^{-2})	b_2 (GeV^{-2})
I	47.5	-	0.		45	38.35	-0.150	0.	-	0.	10.72	-
					301	39.56	-0.008	0.	-	0.	11.76	-
					393	40.05	0.012	0.	-	0.	11.99	-
II(i)	39.379	14.770	1.	this work	45	38.35	-0.150	1.	-0.44	0.42	12.21	7.64
(ii)	44.358	10.445	0.858	/ 9/	301	39.56	-0.008	1.	-0.44	0.31	13.50	6.93
(iii)	42.946	6.136	1.	/ 21 /								

<u>Version II</u>

For this more complex parameterization, many of the details are given in the Appendix. A double Gaussian expression replaces the single Gaussian expression in the nucleon-nucleon amplitude. In addition, ρ, the ratio of the real to the imaginary parts of the nucleon scattering amplitude, is given a t (or q^2) dependence.

The choice of the wave function parameterization is difficult. We have chosen a double Gaussian expression taken from ref. 9, 21 (see Eq. A5 in the Appendix) containing three parameters R_1, R_2 and C. Different values of these parameters were used[9,22,23] to describe the same experimental electron-helium data[5,6]. Usually the efforts to fit better, the position of the minimum and the magnitude of the second maximum of the ^4He form factor were made at the expense of a worse agreement with experimental data in the lower t region. In order to calculate correctly the p^4He differential cross

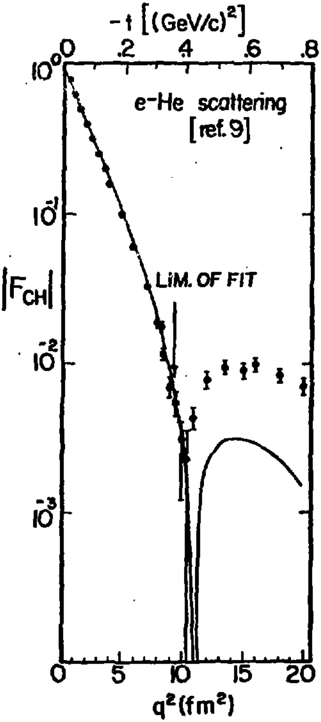

Fig.10. The charge form factor of ^{4}He calculated from the single-particle wave function (A5). The parameters (see Table IX) have been fitted to the data of refs.5,6 for $|t| \lesssim 0.35\ (\mathrm{GeV/c})^2$.

section in the relatively small t-region we obtained new values for the wavefunction parameters from simultaneously fitting the two electron ^{4}He experiments of refs. 5,6 for the limited region $q^2 \leq 9\ \mathrm{fm}^{-2}$ ($|t| \leq 0.36\ (\mathrm{GeV/c})^2$. Our fitted values are $R_1 = 39.4$ fm, $R_2 = 14.8$ fm; $C = 1$ is found in the limit of the constraint $0 \leq C \leq 1$. The result of this e^{4}He is shown in Fig. 10.

In Fig. 11a and b we show the ratio of our Version II curves to the curves of Version I calculated at 45 and 301 GeV respectively. Also shown are two additional curves where alternative parameterizations for the wave function are used; these are the Bassel-Wilkin[5] and the Chou[21] models. The agreement with the data is still not good. The three curves in Fig. 11a, b show the importance of the choice of the wave function parameterization. The discrepancy between the data and theory in the very small t-regions is 10-15%, as contrasted to the 4.8% total normalization error.

If we were to assume that the normalization error is higher than estimated (See Section III) one can try to reach a better agreement (between data and theory) by changing the normalization of the data. The change of the normalization causes a parallel shift of points in a up-down direction on the logarithmic scale of Fig. 11a and b, but the differences in the shape of the curves and the data are still significant.

It is very likely that the major cause of the failure of the Version II parameterizations is the failure to include inelastic intermediate states in the double, triple, and quadruple nucleon rescattering terms. We have not pursued this matter further quantitatively because of the normalization difficulties mentioned previously but do suggest the high energy and the accuracy of our data allow further analysis. Data on non A=1 targets are the only way to study the short range interaction of N* excited nucleon states.

Finally we show the difference between the data and the Glauber model calculation using amplitudes. Let us assume that the correction amplitude, F_{corr}, satisfies the relation

$$\frac{d\sigma}{dt}_{exp} = \left| F_{Glauber} + F_{corr} \right|^2 , \qquad (8)$$

where $\frac{d\sigma}{dt}_{exp}$ is experimental differential cross section. Assuming that

$$\mathrm{Re}(F_{corr}) = 0 \tag{9}$$

one can determine F_{corr} directly from experimental data as

$$F_{corr} = \pm\sqrt{\frac{d\sigma}{dt}_{exp} - \left(\mathrm{Re}(F_{Glauber})\right)^2} - \mathrm{Im}(F_{Glauber}). \tag{10}$$

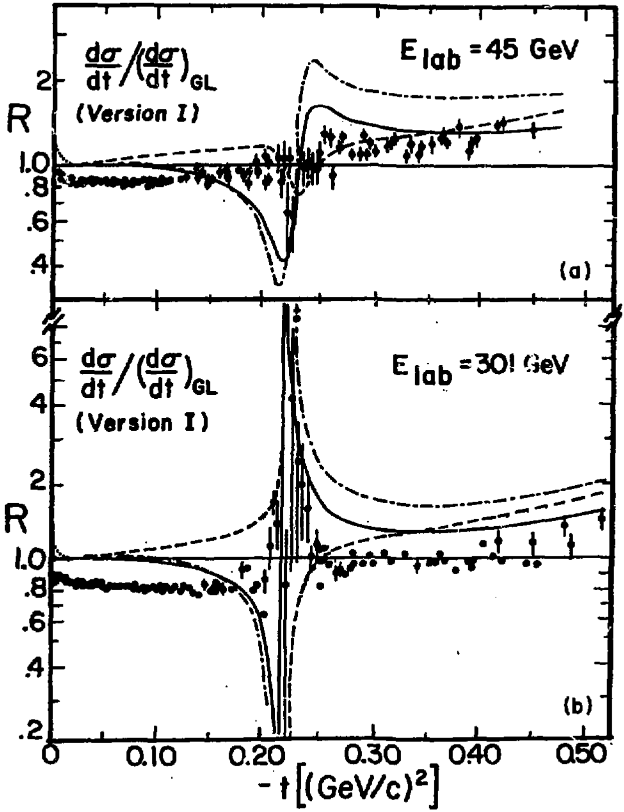

The result is shown in Fig. 12 (only one of two solutions of Eq. (10) is plotted). In the calculation of $F_{Glauber}$ we use the Bassel-Wilkin wave function parameterization (Version II(ii)). The analysis, similar to that made for pd and dd cases[22], suggests that F_{corr} can be interpreted as an interference of rescatterings with intermediate inelastic states.

The inelastic screening correction at $t = 0$ is estimated under the assumption that the discrepancy between the data and the Glauber model prediction is mainly due to this effect. The contribution of the inelastic screening correction, $\Delta\sigma_{in}$, to the total cross section ($\sigma_{pHe} = 4\sigma_{pN} - \Delta\sigma_{el} - \Delta\sigma_{in}$) is $\sim$9 mb which is $\sim$15 times higher than in pd scattering and somewhat higher than the prediction given in ref. 8.

Figure 11: The elastic p^4He differential cross section. All data points have been renormalized to the Version I Glauber model prediction. The curves show the results for various Version II fitting procedures. Inelastic rescatterings are excluded in the analysis; the nucleon-nucleon amplitude is given by (A3). Three one-particle wave function (A5) parameterizations are used:

-.-.-.-.- our values for R_1, R_2, C(II(i)),

———— Bassel-Wilkin (II(ii)), ref. 9,

- - - - - Chou (II(iii)), ref. 21.

These three parameterizations are listed in Table IX. The Coulomb effect in the small t-region is marked with:

. . . . .

(a) E_{lab} = 45 GeV, (b) E_{lab} = 301 GeV.

Fig.12. The Glauber correction amplitude F_{corr} determined from the elastic differential cross section at 45 GeV. The Bassel-Wilkin parameters (ref.9) for the ^{4}He wave function have been used. The points ♦ have negative sign, o - positive sign.

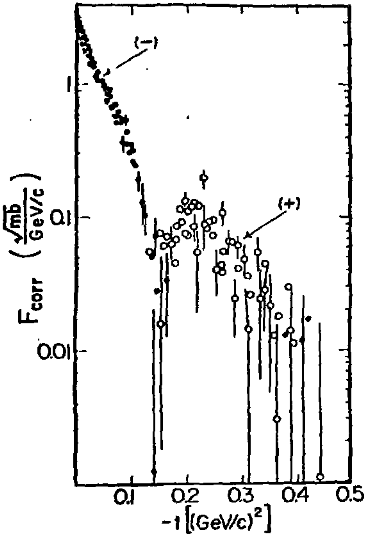

VII. CONCLUSIONS

In this experiment elastic p^{4}He scattering has been investigated in an energy range $45 \leq E_{lab} \leq 400$ GeV. The t-interval $0.003 \leq |t| \leq 0.5$ $(GeV/c)^2$, where the differential cross section has been obtained, comprises the Coulomb interference region, the forward diffraction peak, the Glauber minimum, and the second maximum. It contains about 110-140 data points at each primary proton energy and is measured with a typical relative statistical error of about 1.5-3%, except in the region of the minimum around $|t| \lesssim 0.22$ $(GeV/c)^2$ where errors sometimes reach 50%.

The technique of the mixed hydrogen-helium jet target allows one to obtain absolute normalization of the differential cross section. The optical theorem is used to determine the total cross section for pHe interactions. $\sigma_{tot}(E)$ rises for $E \geq 100$ GeV.

The parameters $\rho(s, t=0)$ and $b(s, t)$ of the pHe scattering amplitude are obtained. The rate of shrinkage of the pHe diffraction cone is more than twice as large as that for pp scattering. Geometrical scaling, $\sigma_{tot}(E)$ proportional to $b(E)$, is satisfied but the other geometrical relation for the height of the second maximum, $\frac{d\sigma}{dt}(E, t_{sec.max})$ proportional to $\sigma_{tot}^2(E)$, is strongly violated.

The analysis of simple forms of the Glauber model show that substantial corrections to the elastic scattering amplitude are needed. Inelastic screening seems to be important in the region of the diffractive cone as well as in the second maximum of the differential cross section. A more accurate estimation of the effect requires a better understanding of ^{4}He wave function.

ACKNO' .EDGEMENTS

We acknowledge the strong support of the Fermilab Internal Target Group led by Dr. Tom Nash, the Accelerator Division led by Dr. Russ Huson, and the Fermilab Computing Department led by Dr. Al Brenner. We are grateful to Professor Vladimir Kadeshevsky for his help. One of us (A. B.) acknowledges Dr. Z. Ajduk and Dr. L. Leśniak for helpful discussions. The Dubna members of the collaboration wish to acknowledge the support and hospitality of the Fermilab Directorate during their stay in the United States. Finally, the authors are grateful to their colleague, Dr. Andrzej Sandacz for his help.

APPENDIX

In this Appendix we show the formalism of the multiple scattering Glauber model and list some of the detailed parameterizations to which we have fitted our data; results are given in Section VI, Tables VIII, IX, Figures 7-12.

Defining the total density of the nucleus as a product of separate nucleon densities

$$= \Psi^*\Psi = \prod_{i=1}^{4} \rho_i(\bar{r}_i) \tag{A1}$$

$$\text{with } \left(\int \rho_i(\bar{r}_i)\, d^3 r_i \equiv 1\right)$$

we derive the nuclear amplitude from the Glauber model:

$$
\begin{aligned}
F(\bar{\Delta}) = {} & 4\, f(\bar{\Delta}) \cdot G\left(\tfrac{3}{4}\,\bar{\Delta}\right) \cdot G\left(-\tfrac{1}{4}\,\bar{\Delta}\right) \\
& - \frac{6\, G^2\left(-\frac{\bar{\Delta}}{4}\right)}{2\pi i p} \int d^2q\, f\left(\tfrac{3}{4}\,\bar{\Delta} - \bar{q}\right) \cdot f\left(\tfrac{\bar{\Delta}}{4} + \bar{q}\right) \\
& \cdot G\left(\tfrac{\bar{\Delta}}{2} - \bar{q}\right) \cdot G(\bar{q}) + \frac{4\, G\left(-\frac{\bar{\Delta}}{4}\right)}{(2\pi i p)^2} \int d^2q_1\, d^2q_2 \\
& \cdot f\left(\tfrac{\bar{\Delta}}{4} + \bar{q}_1\right) \cdot f\left(\tfrac{\bar{\Delta}}{4} + \bar{q}_2\right) \cdot f\left(\tfrac{\bar{\Delta}}{2} - \bar{q}_1 - \bar{q}_2\right) \\
& \cdot G(\bar{q}_1) \cdot G(\bar{q}_2) \cdot G\left(\tfrac{\bar{\Delta}}{4} - \bar{q}_1 - \bar{q}_2\right) \\
& - \frac{1}{(2\pi i p)^3} \int d^2q_1\, d^2q_2\, d^2q_3 \cdot f\left(\tfrac{\bar{\Delta}}{4} + \bar{q}_1\right) \\
& \cdot f\left(\tfrac{\bar{\Delta}}{4} + \bar{q}_2\right) \cdot f\left(\tfrac{\bar{\Delta}}{4} + \bar{q}_3\right) \cdot f\left(\tfrac{\bar{\Delta}}{4} - \bar{q}_1 - \bar{q}_2 - \bar{q}_3\right) \\
& \cdot G(\bar{q}_1) \cdot G(\bar{q}_2) \cdot G(\bar{q}_3) \cdot G(-\bar{q}_1 - \bar{q}_2 - \bar{q}_3).
\end{aligned}
\tag{A2}
$$

The Fourier transform of the one-particle density is

$$G(\bar{q}) = \int e^{i\,\bar{q}\,\bar{r}} \cdot \rho_i(\bar{r})\, d^3r \quad .$$

$\bar{\Delta}$ and $\bar{q}$ are the vectors of the transverse momentum transfers to the nucleus and to the nucleon respectively, p is the laboratory momentum of the projectile, and $\bar{r}_i$ is the position of the i-th nucleon in c.m.system of the nucleus. Formula (A2) contains the constraint associated with the uniform motion of the nuclear center-of-mass.

The amplitude F is normalized as

$$\frac{d\sigma}{dt} = \left|\frac{\sqrt{\pi}}{p} \cdot F\right|^2,$$

where $-t = q^2$.

The nucleon-nucleon amplitude is parameterized in the form

$$f(q) = \frac{\sigma_{tot}}{4\pi} \cdot p \cdot [i + \rho(q)] \cdot \frac{e^{-\frac{b_1}{2}q^2} + \beta \cdot e^{-\frac{b_2}{2}q^2}}{1 + \beta}, \qquad (A3)$$

where σ_{tot} is the nucleon-nucleon total cross section and $\rho(q)$, the ratio of the real to imaginary parts of the amplitude is

$$\rho(q) = \frac{Re\ f(q)}{Im\ f(q)} = \rho(0) + \rho' (e^{\gamma q^2} - 1), \qquad (A4)$$

b_1, b_2, β, ρ, and γ are all arbitrary parameters.

For the one-particle density we take the form of a double Gaussian proposed by Bassel and Wilkin[9], and Chou[21]:

$$\rho_i(\bar{r}_i) = K \left[\exp\left(-\frac{\bar{r}_i^2}{R_1^2}\right) - C \cdot \exp\left(-\frac{\bar{r}_i^2}{R_2^2}\right)\right] \qquad (A5)$$

with $$K = \pi^{-\frac{3}{2}} \cdot \left(|R_1|^3 - C \cdot |R_2|^3\right)^{-1},$$

where K is the normalization factor R_1, R_2, and C are free parameters, which can be deduced from the charge form factor of the ^4He nucleus.

The Gaussian form of Eqs. A3, A4, and A5 has been chosen partially in order to simplify the necessary integrations.

The Fourier transform of Eq. A5 is

$$G(\bar{q}) = \frac{1}{1-D} \cdot \left[\exp\left(- \frac{R_1{}^2 q^2}{4}\right) - D \cdot \exp\left(-\frac{R_2{}^2 q^2}{4}\right)\right] \qquad \text{(A6)}$$

with $\quad D = C \cdot (R_2/R_1)^3$.

Inserting Eqs. A3 and A6 into Eq. A2 we may calculate the differential cross section in two ways:

<u>Version I</u>

$$\beta,\ D,\ \rho' = 0$$

In this case the amplitude F (Eq. A2) takes a well known form.[19] The parameters $b = b_{pp}$ $\rho = \rho_{pp}$ $(t = 0)$, and $\sigma_{tot} = \sigma_{tot}^{pp}$ are fixed by pp experiments [14,18] or treated as variable parameters. The parameter $R_1 = 1.36$ fm.[23]

<u>Version II</u>

A more realistic version for calculation is to take into account more complex expressions for the nucleon-nucleon amplitude and a more realistic expression for the charge form factor of ^{4}He nucleus.

The parameters β, b_1, b_2 of the elementary amplitude have been determined as follows:

(i) The experimental pp data have been interpolated to our energies using the known[19, 24] energy dependence of the parameters.

(ii) The reconstructed differential cross sections have been fitted using our parameterization (A4) with fixed values of $\rho' = 1$, and $\gamma = -0.44\ (\mathrm{GeV/c})^2$. We have assumed here that the amplitude ratio (A4) is approximated as

$$\rho(t) = \frac{\mathrm{Re}\ f(t)}{\mathrm{Im}\ f(t)} = \rho_o^{pp}\ (s,t=0) + \frac{1}{2}\pi \left[\alpha_{\mathrm{Pomeron}}(t) \ -1\right] \quad \text{(A7)}$$

$$\cong \rho_o^{pp} + 0.44\ t \cong \rho_o^{pp} + (e^{0.44t} - 1),$$

where $\alpha_{\mathrm{Pomeron}} = 1 + 0.278\ t$.

REFERENCES

1. See e.g. review by G. Igo in High Energy Physics and Nuclear Structure, p. 63, Proceedings of the Santa Fe conference, published by American Inst. of Physics (1975).
2. J. Berthot et al, Clermont-Ferrand, Lyon, Stasbourg collaboration, preliminary results as reported at various conferences, e.g., Proceedings of the conference on High Energy Physics and Nuclear Structure, Uppsala, 1973.
3. V. Avdeichikov, Soviet Journal of Nucl. Phys. 27, 710 (1978).
4. V. G. Ableev et al.,Communication of the J.I.N.R., P1-10565, Dubna (1977).
5. R. F. Frosch et al., Phys. Rev. 160, 874 (1967).
6. F. C. McCarthy et al., Phys. Rev. 15C, 1396 (1977).
7. T. Ekelöf et al., Nucl. Phys. B35, 495 (1971).
8. E. M. Levin and M. I. Strikman, Leningrad Nuclear Physics Institute, Report 203 (1975).
9. R. Bassel and W. Wilkin, Phys. Rev. 174, 1179 (1968).
10. W. Czyż and L. Leśniak, Phys. Lett. 24B, 227 (1967).
11. W. Czyż and L. C. Maximon, Phys. Lett. 27B, 354 (1968).

12. J. Auger et al., Nucl. Phys. A262, 372 (1976).

13. A. Bujak et al., "Coherent Diffraction Dissociation of Helium from 46 to 400 GeV." Phys. Rev. D, following paper.

14. A. S. Carrol et al., Phys. Rev. Lett. 33, 928 (1974).

15. Schiz et al., to be published in Phys. Rev. D.

16. J. P. Burg et al, "Measurements of the total π-He and p-He cross sections and the slopes of the forward diffraction peak at energies from 50 to 300 GeV." Preliminary results presented at the 20th International Conference on High Energy Physics, Madison, USA, July 1, 1980.

17. E. Jenkins et al, "Proton-Helium Elastic Scattering from 40 to 400 GeV." Preliminary results from this experiment presented at the 19th International Conference on High Energy Physics, Tokyo, August 1978. Also quoted in rapporteur talk by V. A. Nikitin "Soft Hadron Reactions" published in the proceedings of the European Physical Society Conference, Geneva, 1979 p. 547-567.

18. H. Bethe, Ann Phys. (N.Y.) 3, 190 (1958).

19. D. Gross et al., Phys. Rev. Lett. 41, 217 (1978).

20. Yu. Y. Azimov et al., JETP Lett. 23, 131 (1976).

21. T. T. Chou, Phys. Rev. 168, 1594 (1968).

22. G. Goggi et al., Nucl. Phys. B149, 381 (1979).

23. E. Lambert and H. Feshbach, Ann. of Phys. 76, 80 (1973), p. 102.

24. D. S. Ayres et al., Phys. Rev. 15D, 3105 (1977).

Received by Publishing Department
on April 28 1981.